ARTICLES

Ions in Crystals: The Topology of the Electron Density in Ionic Materials. III. Geometry and Ionic Radii

A. Martín Pendás,* Aurora Costales, and Víctor Luaña

Departamento de Química Física y Analítica, Facultad de Química, Universidad de Oviedo, E-33006-Oviedo, Spain

Received: January 27, 1998

We present the application of Bader's topological analysis of the electron density to geometric properties in ionic materials. Particular attention is paid to the concept of ionic radius, in relation to the shapes of ions in crystals, and to the various correlations among atomic properties, i.e., electronegativities, deformabilities, etc., that it induces. Using a simple model to fit our results to a theoretical frame, we show that ionic bonds display properties in complete parallelism to those known in covalent bonds. This allows us to define unambiguosly the strength of an ionic bond, which is found to correspond to Pauling's bond valence.

1. Introduction

The development of the physics and chemistry of the solid state has been intimately linked to the vague concept of atomic size. In the context of ionic materials, where it was first recognized, it has played a primary role through the years. In our day, it is still the very first concept invoked when trying to rationalize both experimental and theoretical results. However, besides their proven power of systematizing observations, ionic radii have probably reached their present status because they geometrize solids, creating clear and easy to comprehend pictures of reality. Through the years, a vast amount of information regarding radii and their variation, usefulness, or uselessness has been gathered, and literally hundreds of methods to obtain radii from experiments or theory have been proposed.

The first sets of ionic radii were those of Landé[1] and Wasastjerna.[2] Both used X -ray crystal data and additional hypotheses (halogen contact in lithium salts and proportionality of polarizabilities to atomic volumes, respectively) to extract individual ionic radii from experiment. Soon afterward, Goldschmidt,[3] Pauling,[4] and Zachariasen[5] extended and improved these early values. All of them introduced more or less theoretical assumptions, of which Pauling's criterion of inverse proportionality between effective nuclear charges and ionic sizes may be considered a prototype. Further developments[6,7] avoided these criteria, introducing energetic models of the lattices and new empirical, nongeometric data. These proposals tried to solve the problem posed by how to partition single geometric data (lattice parameters) among plural entities (cations and anions). From today's point of view, it is apparent that these arbitrary recipes do not face the very root of the problem: the division of physical space into atomic regions. The success of ionic radii was, nevertheless, tremendous. Pauling's[8] ratio of cation to anion radii (i.e., radius ratio) was able to offer, for the first time, a consistent structural coordinate to rationalize the preference between the rock-salt (B1) and the cesium chloride (B2) phases. Pauling's rules[9] reinforced this success even further.

The first major revision of the crystal radii was made in the first 1960s, when Fumi and Tosi[10] criticized Pauling's criterion. They recognized that the effective charges used in those days were almost those of free ions and thus were not suited to obtain crystalline results. Moreover, all other radii sets were influenced by this fact in one way or another. The new ionic radii they obtained were fully thermochemical, with quite larger cations and smaller anions than those of Pauling's. On the other hand, the first reliable electron density maps for NaCl[11,12] gave points of minimum density along the internuclear axes (empirical radii) in good agreement with Fumi and Tosi's radii, and not with Pauling's. As soon as good densities from X -ray diffraction became available, new compilations of mixed X-ray and thermochemical radii, like the one of Shannon and Prewitt,[13] appeared.

Since then, one stream of work has generated more and more specific radii, dependent on the valence and the coordination state, the family of compounds, etc. Better thermodynamical data have been used to reconstruct Fumi−Tosi's tables,[14] confirming an ever growing tendency toward larger cations, smaller anions, and larger size variability, with respect to Pauling's radii. When in recent years accurate electron densities have been measured all over a unit cell,[15−18] they have served to prove that an ion may display different radii along different directions. Perturbing but interesting enough is the finding by Downs and Swope[19] that these directional radii tend to the known ionic radii of their corresponding coordination indices. From all these data O'Keeffe[20] concludes that tables of crystal and ionic radii have little significance except as generators of average bond lengths. Soon, even the ability to make structural predictions based upon radii became suspect. It was proved, for example, that the cation to anion size ratio failed to ascribe correctly the stable phase (B1 or B2) in half the alkali halides.[21] Even so, the original rules of Pauling have been improved through more and more elaborated recipes for the bond-valence concept,[22,23] being now widely used in inorganic and crystal chemistry.

On the other hand, a completely new set of size coordinates were discovered when first-principles techniques and, particularly, pseudopotential theory acquired a mature state.[24] Zunger,[25] in a shocking paper, used angular momentum dependent orbital

S1089-5647(98)00906-7 CCC: $15.00
Published on Web 08/15/1998

radii, defined as the distance at which the *l*-screened pseudopotentials for free atoms vanished, and used them as structural coordinates extending the works of Simons and Bloch,[26] St. John and Bloch,[27] and Machling, Chow, and Phillips.[28] This radii, characterizing a "size" for an atomic core, displayed very clear periodic variations and correlations almost with any atomic or ionic property. Clever combinations of *s*- and *p*-type radii for binary compounds were able to isolate clear and easy to plot phase stability regions for all the known crystalline binary compounds and to predict the heat of formation of metal alloys.[29] The scheme was later developed and applied to separate more than 3000 intermetallic compounds with almost full success,[30] and even simplified on realizing that just the *s*-orbital radii were really necessary to obtain almost full predictive power.[31] Orbital radii have very recently drawn the attention of chemists, and through modern density functional ideas a new scale of radii has been constructed and successfully related to electronegativity, polarizability, and several other atomic and bonding properties.[32] Finally, many other types of orbital radii, like Bucher's[33,34] orbital moments method, have been proposed. All of them share one property. They mix geometric parameters with energetic ones (orbitals), and their predictive performance should not be compared with that of purely geometric entities.

In our opinion, many of the unsatisfactory characteristics associated with the ionic radius concept emanate from its rather slippery definition in quantum mechanics. Bader's theory of atoms in molecules (AIM)[35] provides the definitive frame in which to assign an accurate meaning to geometric coordinates in solids. In a condensed phase, an AIM atom (or ion) is a closed region of the physical space, having well-defined boundaries and volume. In our two previous papers,[36,37] we have applied the AIM theory to periodic solids, undertaking a systematic analysis of the topology of the electron density in these systems. We have found several fundamental properties not previously explored, like the isomorphism between an AIM atom and a convex polyhedron, and we have also examined the whole series of alkali−alkaline earth−halide perovskites. In this third paper we study the unambiguous size coordinates arising from an AIM description of the electron density in ionic materials, particularly the B1 and B2 phases of the alkali halides and the above-mentioned perovskites. It is our basic aim to show how once the ionic radius concept is stripped of the requirement of immutability and predictive character in the phase stability problem, a new wealth of behavior may be uncovered. When radii are seen again as purely geometric entities, many of our old intuitions acquire a renewed meaning.

We have structured the paper as follows: In section 2 we will briefly introduce the method followed, paying special attention to the various problems posed by the accuracy of theoretical geometries, basis set effects on the density, etc. Section 3 will be devoted to the study of the relation between lattice geometry and the topology of the electron density, choosing the alkali halides as an example. We will introduce here some interesting findings, like topological isomerization induced by pressure. In section 4 we will examine the AIM ionic radii for our model compounds and will introduce a simple model that is able to explain a whole series of behaviors. Section 5 will present a flavor of the correlations that may be found between our radii and other properties such as the electronegativity, the ionic deformability, etc. Finally, we will summarize our conclusions and give some prospects in section 6.

2. Method

Our first goal is to obtain good-quality electron densities for a whole series of ionic compounds for use in the topological analysis. As in our previous work, we have used the ab initio perturbed ion method (aiPI),[38−40] a localized quantum mechanical Hartree−Fock (HF) scheme that has been used extensively to describe accurately the electronic structure of ionic and partially ionic pure and defective solids. The densities obtained through this procedure have been the input to the CRITIC program,[41] a code that automatically searches for all the independent critical points in a crystal lattice. It does so by means of a recursive division of the irreducible wedge of the Wigner−Seitz polyhedron of the Bravais lattice. The code also obtains the zero-flux atomic (ionic) surfaces and several observables integrated in their basins. It allows in this way for systematic (and automatic) AIM investigations in pure crystals.

When trying to study only the broad topological features of a system, like the topological class or scheme to which the system belongs,[37] one may ignore many of the subtle differences in the computed densities coming from the fine tuning of the parameters entering the calculations. The topology of the electron density scalar field is structurally stable in almost every situation, far from bifurcation points. However, if our aim is to compare geometric or energetic observables induced by the topology with empirical analogues, as in the case posed by ionic radii, particular care must be taken. It is necessary then to examine the dependence of the observables on computational parameters.

In our present work, the computed electron densities depend mainly on two types of variables: (i) the lattice geometries and (ii) the basis sets used to represent the localized atomic (ionic) wave functions. As the first point is concerned, the theoretical equilibrium observables (lattice parameters, lattice energies, elastic constants) obtained with the aiPI method are usually within 5% of experimental results.[40] This precision is very reasonable, but when examining tendencies, the systematic errors coming from relativistic effects, inaccurate estimation of the correlation energy corrections (CEC),[42] etc., degrade the relations among properties to some extent. We have tried to minimize these phenomena by using a 2-fold strategy. High-accuracy calculations, like those in the alkali halides, have been performed at several computational levels (HF, HF+CEC) at both theoretical and experimental geometries. Our fine arguments about the behavior of radii will be mainly based on the densities obtained at the experimental geometries.[43] On the other hand, given the scarce number of perovskites actually synthesized out from the 120 compounds studied, we will use their theoretical equilibrium distances to obtain their electron densities and will use these data to discuss coarse-grained features of their ionic radii. As regards the second point, we have used generally, as in previous works, the multi-ζ exponential basis sets of Clementi and Roetti (CR).[44] The recent availability of the excellent quality basis sets of Koga, Watanabe, Kanayama, Yasuda, and Thakkar (KWKYT),[45] which, for the ions of interest, are within 9 μhartree from the HF limit, has allowed us to use another reference. We have been surprised by the "low" quality shown by the CR basis in the ^{1}S states of the heaviest ions, with energies away the HF limit as much as 13 mhartree in the I^-. This fact may be at the core of the degradation process observed in the aiPI results in compounds wearing heavy ions. The influence of the basis in the final observables is, however, rather low. A geometry optimization with the KWKYT basis in the alkali halides at the HF level gives rise to equilibrium geometries that agree within 5%

agreement of those obtained with the CR basis, except for the case of CsF. In the latter, the KWKYT basis gives $a = 11.63$ a_0, in much better agreement with experiment ($a = 11.34$ a_0[43]) than $a = 10.61$ a_0, obtained with the CR basis. On the other hand, if both basis sets are compared at a given constant lattice parameter, the resulting ionic radii differences are controlled by the anion, with CR fluorides 0.3% too small with respect to the KWKYT results, chlorides 0.4% too big, bromides 0.1% too small, and iodides 0.7% too small, respectively. In our opinion, these differences are negligible, and in the following we will restrict to our usual CR data, except when explicitly stated.

We therefore performed aiPI HF and HF+CEC geometry optimizations of the B1 and B2 phases of the 20 common alkali halides, plus single-point computations at their experimental geometries. We have also used the HF+CEC optimized geometries of the 120 perovskites described in paper 2 and of the 20 alkaline earth−halide fluorites. The rest of our discussion is based on the topological analysis of these electron densities.

3. Radii as the Topological Organizers

The alkali halides display two of the most simple crystal structures, the B1 and B2 crystalline phases, and are known to undergo pressure- and temperature-induced transitions from the one to the other. They have therefore been particularly suited for theoretical as well as experimental investigations. The same may be said as the topology of the electron density is regarded. We will briefly review in this section the topological schemes shown by the alkali halides in both phases, studying the connection between these schemes and bonded radii. From now on, we define the concept of ionic *radius* as the (direction-dependent) distance from one nucleus to the limit of its atomic (ionic) basin. A bonded radius is then a radius along a (nonambiguous) bond direction. It is to be understood, therefore, that a given nucleus may display different bonded radii if bonded to more than one nonequivalent species.

A. Topology in the B1 Phase. We have found three different topological schemes in the B1 phase of the alkali halides. Using the *nbrc* notation introduced in paper 2, which concisely states the number of nonequivalent nuclei (*n*), bond points (*b*), ring points (*r*), and cage points (*c*), they are described as (2111), (2211), and (2222), or as the R_1, B_1, B_2 families. If we place the cation at the 4*a* Wyckoff position (0, 0, 0), and the anion at the 4*b* one ($^1/_2$, 0, 0) when constructing the unit cell, the 8*c* position is always a *c*-point. The only other fixed point of the $Fm\bar{3}m$, space group, the 24*d* point at ($^1/_4$, 0, $^1/_4$), discriminates between the *R* and the *B* families, being an *r*-point in the former and a *b*-point in the latter. In this way, the R_1 scheme has only cation−anion bonds, displaying the usual six−six coordination, while the *B* families show also anion−anion bonds and 6−18 coordination. A summary of the critical point information for the three schemes appears in Table 1.

At the HF+CEC optimum geometries, the R_1 family is the most numerous, being represented by all the cesium halides and KCl, NaF, KF, RbF, RbBr, and RbCl. The B_1 scheme is shown in the KI, KBr, LiF, RbI, NaBr, NaCl, and NaI, crystals and the B_2 family in LiI, LiCl, and LiBr. At this level it is already notable that the radius ratio may be controlling the topology of the crystals. To gain some insight into the reasons behind this idea, it is useful to visualize prototypes of the atomic basins for every topological family. These are plotted in Figure 1. We can easily see how the cations are always homomorphic to a cube, actually a bumped cubed, and that the anions are also cubes in the R_1 family or edge-truncated cubes (ETC's) in the *B* families. It is also to be noticed that B_1 cations show peculiar spikes that connect the cationic basins to the single class of 8*c* cage points present in the structure. The spikes should be familiar after our arguments in paper 2, and point toward the cage points that constitute the vertices of both the anionic and the cationic faces.

TABLE 1: B1 Topological Families and Their Nonequivalent Critical Points[a]

Wyckoff position	generator	R_1	B_1	B_2
48*h*	(0, *y*, *y*)		*r*	*r*
32*f*	(*x*, *x*, *x*)			*c*
32*f*	(*y*, *y*, *y*)			*r*
24*e*	(*x*, 0, 0)	*b*	*b*	*b*
24*d*	(0, $^1/_4$, $^1/_4$)	*r*	*b*	*b*
8*c*	($^1/_4$, $^1/_4$, $^1/_4$)	*c*	*c*	*c*
4*b*	($^1/_2$, $^1/_2$, $^1/_2$)	*n*	*n*	*n*
4*a*	(0,0,0)	*n*	*n*	*n*

[a] For each family we specify the type of critical point present at each Wyckoff position. The notation *n*, *b*, *r*, *c* refers to nuclei, bond, ring, and cage points, respectively.

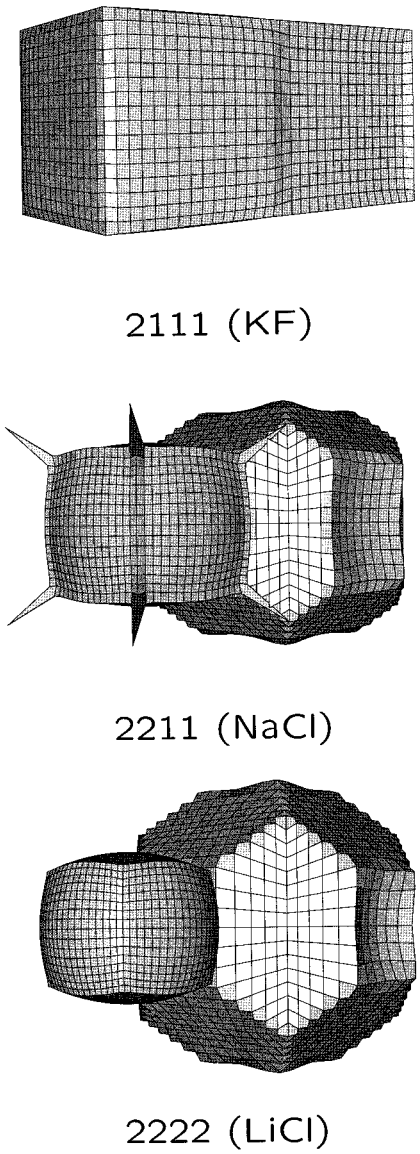

Figure 1. Prototypical ionic basins for the three topological families in the B1 phase of the alkali halides. In each plot, the small basin corresponds to the cation and the larger one to the anion. The pictures have been created with TESSEL[53] and rendered with GEOMVIEW.[54]

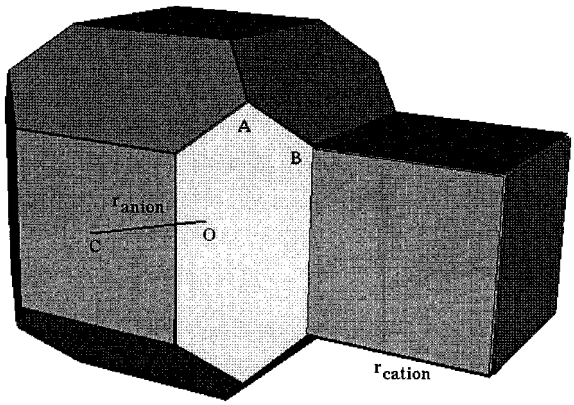

Figure 2. Generic-weighted proximity polyhedra for a pair of adjacent ions in the B1 alkali halides.

If we neglect face curvature and spikes in the basins, the weighted proximity polyhedra (WPP) are extremely good approximations to the actual ionic shapes. Figure 2 shows the generic WPP of the B1 alkali halides. It is completely determined by the values of r_a and r_c, being r_a the radius of the cube in which the ETC may be inscribed. If r_c converges toward r_a, the anionic polyhedra collapses onto a cube. If r_c tends to zero, the anion becomes a regular ETC. We see, therefore, that all of the shapes actually displayed by the crystals are well-defined cases of our generic WPPs. Moreover, it is clear from this analysis that there should be a clear tendency toward the two-cube, R_1 family as the cationic radius tends to the anionic one, as presently found. Though this topology should ideally be found only for strictly identical ions, the nonplanarity of faces and other effects should introduce a range of stability for the R_1 scheme around $r = 1$. As the *B* families are concerned, it is easily verified that point A in Figure 2 is necessarily the 8*c* cage point position and that the AB line, if continued into the cationic cube, is one of its diagonals and, therefore, the (*x*, *x*, *x*) crystallographic direction. This means that in the B_1, B is not a critical point but rather extends a spike toward the A point.

In the B_2 family, the B point is a *c*-point, and a new ring emerges between the AB segment. Why do there exist two *B* families? It seems that for *r* values that are not too small, the appearance of spikes in the atomic basins avoids the formation of a new cage + ring pair near the B point. This situation can no longer be sustained for really small *r* values. An indication of the origin of this behavior may be found in the "basins of repulsion representation" rather than in the present "basins of attraction representation". In the former, the coordination polyhedron of a *B* cation is an octahedron, whose triangular faces are rings of anion−anion bonds. If a ring point is to exist at the center of one of these triangles and we explore the planar face situation first, its crystallographic position must be exactly ($^1/_6$, $^1/_6$, $^1/_6$). It is to be noticed that this relation is fulfilled extremely well by our data—i.e., (0.1669, 0.1669, 0.1669) in LiCl—in the B_2 family. This shows that *ring stress*, pulling a ring out of the geometrical plane in which it should ideally sit, is a particularly undesirable topological feature. With these facts in mind, a constraint between ionic radii is apparently necessary for the B_2 family to exist. For along the (*x*, *x*, *x*) direction, the cage point marking the end of the cation, at a gross distance λr_c, $\lambda = \sqrt{3}$, from the nucleus, must be found *before* the ring point at $(1/\sqrt{3})(r_c + r_a)$, so $r_a/r_c = 1/r > \lambda\sqrt{3} - 1 = 2$. Actually, the cubic shape of the cations is slightly barrel-like, curving itself inward around the vertexes and making $\lambda < \sqrt{3}$. In the cases explored, this value is in the vicinity of $\lambda = 1.3-1.4$. We expect, then, an anion to cation limiting ratio smaller than 2. On the other hand, if there were large enough cations, the situation would be reversible with respect to an exchange of the anion and cation roles, with two other possible *B* topologies with cation−cation bond. We will study this interesting possibility in the B2 phase.

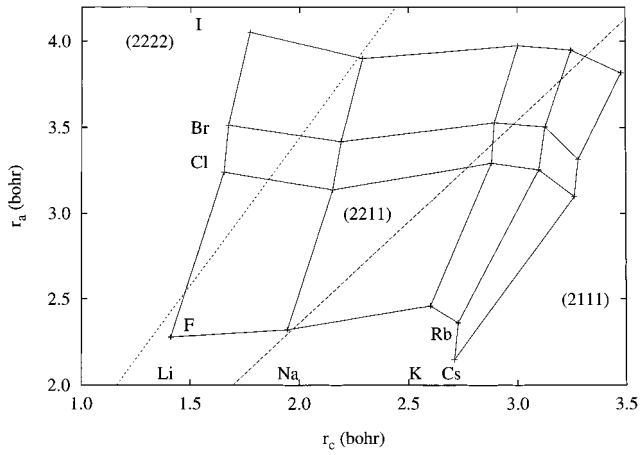

Figure 3. Classification of the topological families ((*nbrc*) notation) of the B1 alkali halide crystals at their HF+CEC geometries in a bonded radii plot. Particular crystals are easily identified from the labels. The dotted line separating the (2222) from the (2211) family is $r_a/r_c = 1.72$, while the dashed one dividing the (2211) from the (2111) basins is $r_a/r_c = 1.15$.

TABLE 2: B2 Topological Families and Their Nonequivalent Critical Points

Wyckoff position	generator	*C*	*R*	*B*
12*j*	($^1/_2$, *x*, *x*)			*r*
12*i*	(0, *x*, *x*)	*r*	*r*	*r*
12*h*	(*x*, $^1/_2$, 0)			*c*
8*g*	(*x*, *x*, *x*)	*b*	*b*	*b*
6*e*	(*x*, 0, 0)		*c*	
3*d*	($^1/_2$, 0, 0)	*c*	*r*	*b*
3*c*	(0, $^1/_2$, $^1/_2$)	*b*	*b*	*b*
1*b*	($^1/_2$, $^1/_2$, $^1/_2$)	*n*	*n*	*n*
1*a*	(0, 0, 0)	*n*	*n*	*n*

We have found, then, that in the case of strictly planar faces and ideal polyhedra, that radius ratio controls the appearance of topological schemes. Figure 3 shows the topological families displayed by the B1 alkali halides at the HF+CEC optimal geometries. It shows how structures belonging to the three families tend to cluster together. There are constant r_a/r_c lines that isolate each family. The position of these separating lines has been adjusted by performing calculations at different geometries, not shown in the plot. We see that the actual r_a/r_c ratios are similar, though significantly different, from the ideal theoretical branching ratios, 2 and 1. Nonplanarity of the faces of the atomic basins play, therefore, an important role in the determination of the topology. We have not found yet a successful explanation to the constancy of the nonideal branching ratios.

B. Topology in the B2 Phase and Color Topological Groups. The B2 topologies show the same general trends found in the B1 crystals, and we will only discuss their more relevant features. There are three different topologies, (2211), (2221), and (2321). If we place the cations and anions at the (0, 0, 0) and ($^1/_2$, $^1/_2$, $^1/_2$) positions, respectively, they differ mainly in the character of the 3*d* fixed critical point. It is a ring in the (2221) or *R* family, a cage in the (2211) or *C* family, and a bond in the (2321) or *B* family. Table 2 summarizes the critical point information.

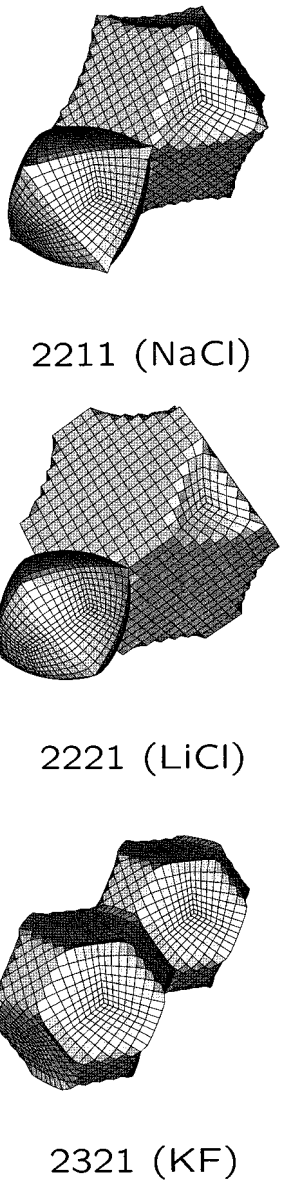

Figure 4. Prototypical ionic basins for the three topological families in the B2 phase of the alkali halides. In each plot, the small basin corresponds to the cation and the larger one to the anion. The pictures have been created with TESSEL[53] and rendered with GEOMVIEW.[54]

The distribution of crystals among families is as follows at the HF+CEC geometries. NaI, LiI, LiBr, and LiCl belong to the *C* family; LiF, NaBr, KBr, KI, RbI, KCl, NaF, and NaCl to the *R* scheme; and KF, RbCl, RbBr, RbF, CsBr, CsCl, CsI to the *B* one. Both the *R* and *C* families show a 8−14 anion−cation coordination, while the *B* family displays a 14−14 coordination, with simultaneous cation−anion, anion−anion, and cation−cation bonds. This is the first topological structure we have found with full connectivity. Prototype ionic basins for each family are shown in Figure 4. We see that now cations and anions are isomorphic to several types of truncated octahedra. We can also observe that the *B* family displays equivalent polyhedra for cations and anions, being like the *R* scheme of the B1 phase, characteristic of similarly sized ions. In the same way the *C* family is equivalent to the B_1 scheme in B1 crystals, and the B2 *R* scheme to the B1 B_2. It is to be noticed that topological complexity (in the sense of greater number of independent critical points) increases in the B1 phase when the cation to anion radii ratio decreases, while the contrary is true for the B2 structure. However, similarly sized anions

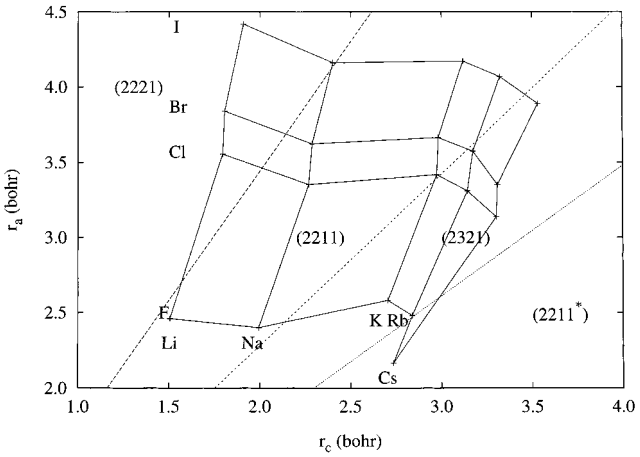

Figure 5. Topological families of the B2 alkali halide crystals at their HF+CEC geometries in a bonded radii plot. Particular crystals are identified as in Figure 3. The long-dashed line separating the (2221) from the (2211) family is $r_a/r_c = 1.72$, the short-dashed one dividing the (2211) from the (2321) basins is $r_a/r_c = 1.15$, and that dividing the (2321) from the (2211*), $r_a/r_c = 0.87$.

are associated in both structures to equivalent polyhedra for both types of ions.

It is possible to undertake a study of the generic WPP as we did previously, with similar conclusions. The ideal *r* ratio controls the topological scheme rigidly, face nonplanarity playing the same softening role as before. Figure 5 shows the bonded-radii classification of the topological families in this structure. It is interesting to note that CsF, which in a first analysis was classified as a (2211) system, lies completely out of its family window. On a closer analysis, we discovered that the topology is actually an inverted (2211) scheme. The cesium cation is so large compared to the fluoride anion that, as far as topology is concerned, it plays the role of the anion. Therefore, in this system there are not cation−anion and anion−anion bonds, but the latter have been substituted by more exotic cation−cation topological bonds. The topology is exactly isomorphic to that of the other (2211) systems by exchange of anions and cations. If we color cations and anions differently, we have found color topological groups in crystalline structures. In this way, if we consider this color group as a new topology, say (2211*), CsF forms itself a new family clearly separated from the rest by a line with exactly the inverse of the slope ($r^* = 1/r = 0.87$) that separates the (2211) from the (2321) families. This result is particularly important, since it shows the consistency of the treatment and the existence of a rather narrow range for a (2321) structure with identical cationic and anionic polyhedra to exist. All the other families should be found in colored versions if sufficiently large cations were found. We also predict a (2211*) B1 family in the vicinity of CsF.

It is also interesting to observe that the branching ratios in both phases may be made to coincide. We have not been able to rationalize this behavior, but we feel that some yet unknown underlying physical feature is responsible for this remarkable coincidence.

C. Topological Isomery. The results of the last section show that there are clear boundaries in the bonded radii space among the different topological families in both the B1 and the B2 phases. As ionic radii must necessarily vary as the lattice parameter of a given crystal is changed, it seems rather sensible that a crystal may undergo a topological transition as the lattice is compressed or expanded. In the AIM chemical language, a change in the network of bonds of a molecule is associated with a change in *molecular structure*. If only a redistribution of the

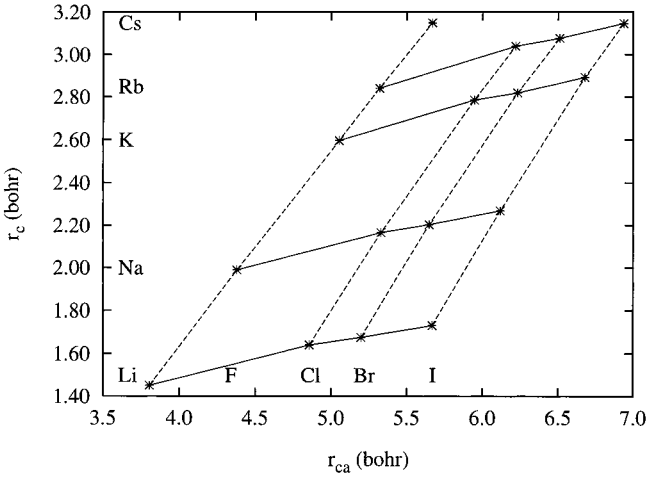

Figure 6. Evolution of the cationic radii of the B1 alkali halides (r_c) with cation−anion bond distance ($r_{ca.}$) at the experimental geometries. Constant cation and anion lines are shown full and dashed, respectively.

bonds occurs, without new isolated species appearing, the process is called an *isomerization*.

We have investigated this issue in those alkali halides that are particularly near the branching ratios in our HF+CEC diagrams: NaI, NaF, and KCl for the B1 phase and RbBr in the B2 structure. We have actually found that at the HF optimum geometries (larger in every case) NaI has changed from (2211) to (2222), KCl from (2111) to (2211), and RbBr from (2321) to (2211). These changes correspond to an artificial expansion from the static equilibrium geometries and are not very relevant except if we try to understand them as simulating temperature in a quasiharmonic way. However, NaF suffers a genuine transition when passing from a lattice parameter $a = 8.53$ a_0 at static equilibrium to $a = 8.35$ a_0. If we use our previously theoretical equation of state for this crystal,[40] we find a transition from the (2111) to the (2211) topology at around 2 GPa. It seems, then, that pressure-induced isomerizations in solids are not also possible, but very likely to occur in the solid state. The relevance of this finding needs further investigation to be fully established and will be one of the items studied in upcoming papers of the series.

4. Ionic Radii and the Exponential Tail Model

The aim of this section is to study the particular radii resulting from the AIM analysis of the alkali halides, along with their behavior and that of other topologically related properties across the periodic table. A careful examination of some characteristics of the radii and electronic densities at the bond critical points will guide us to propose a very simple yet extremely useful model that is able to account for most of our findings. To avoid problems with using theoretical geometries, as described in section 2, we will always use experimental equilibrium geometries.[43] To keep the discussion succinct, we will focus mainly on the B1 radii. This means that all the cesium salts but CsF will be excluded from the analysis. No loss of generality has been found by including CsCl, CsBr, and CsI at their theoretical equilibrium values, but for the sake of consistency, we will not present them.

A. Radii Variations and Empirical Findings. A first rather surprising relation is found on plotting the cationic radii along the cation−anion bond (r_c) versus the cation−anion bond length (r_{ca}). Figure 6 shows that both the cationic and an ionic radii are proportional to the bond distance, with slopes quite independent of the cationic or anionic species. In this way, the cation in the iodide salts is 0.28−0.30 a_0 greater than in the fluorides. The last range determines the cationic size increase in going from Li^+ to Rb^+. The anions show a similar trend, being 0.12−0.09 a_0 greater in the rubidium salts than in the lithium ones. This proportionality between radii and bond distances has been previously observed[46] and is used by those who affirm the uselessness of the ionic radii concept to justify their assertion.

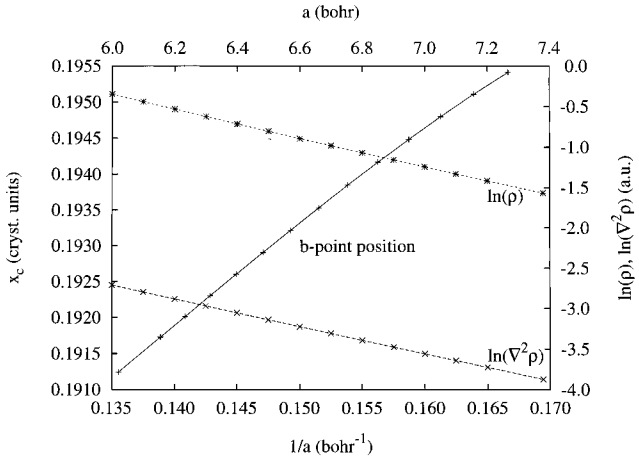

Figure 7. Cation−anion *b*-points, densities, and Laplacians of the densities in the B1 LiF crystal at several lattice parameters. Bond point position (in crystallographic units) is shown in the bottom-left axes with + symbols versus 1/*a*. The logarithms of the density (* symbols) and of the Laplacian of the density (× symbols) are shown in the top-right axes versus *a*.

Not only the particular geometry observed is interesting but also the properties displayed at the cation−anion *b*-point. Figure 7 shows that the crystallographic *b*-point coordinate in the B1 phase of the LiF crystal scales linearly with the inverse of the lattice parameter, meaning that as pressure increases the cation to anion radius ratio (r) gets larger. This view is in complete agreement with the intuitively smaller compressibility of cations. The relation was also observed extremely well (with correlation coefficients greater than 0.999) for a wide range of lattice parameters in all the ionic systems examined. Figure 7 also demonstrates that both the electron density and its Laplacian at the *b*-point are purely exponential functions of the lattice parameter (linear logarithms with regression coefficients greater than 0.999). This is also fulfilled in every crystal studied. Moreover, the slopes found in the fitting are almost identical.

B. The Tail Model. Ionic crystals have been understood for years in terms of almost nonoverlapping ionic densities; we can clearly make the assumption that in the bonding regions the electron density is mainly determined by the tail of the ions. It is also very well-known that an atomic wave function behaves as an exponential at large distances from the nucleus. These ideas are brought together in the following model: along a bond line, at a point x far removed from either nucleus, the electron density is the sum of exponential contributions centered at each of bonded nuclei. If anion B is at a distance r_{ca} from cation A

$$\rho(x) = ae^{-\alpha x} + be^{-\beta(r_{ca}-x)}, \quad 0 \ll x \ll r_{ca} \tag{1}$$

where a, α, and b, β are constants characteristic of the A and B ions in the AB pair, respectively.

Within this model, the position of the bond critical point may be determined by solving for the point x where $\rho(x)$ is a minimum. The result is

$$x_b = \frac{1}{\alpha+\beta}\ln\frac{a\alpha}{b\beta} + \frac{\beta}{\alpha+\beta}r_{ca} \tag{2}$$

TABLE 3: Parameters of the Tail Model in the B1 Alkali Halides[a]

system	a	α	b	β	t_1	t_2
LiF	14.016 72	5.367 31	7.532 93	2.761 98	0.1581	1.8236
LiCl	13.346 61	5.266 26	10.185 21	2.352 36	0.1413	1.6260
LiBr	19.280 29	5.508 39	9.230 77	2.145 69	0.2194	1.5442
LiI	24.869 55	5.645 16	9.104 28	1.958 33	0.2714	1.4540
NaF	27.916 55	4.196 52	6.094 11	2.666 12	0.2879	1.6303
NaCl	26.403 27	4.149 62	7.182 61	2.233 77	0.3010	1.4521
NaBr	35.199 81	4.297 72	6.128 25	2.022 81	0.3958	1.3754
NaI	41.749 09	4.372 15	5.674 19	1.832 84	0.4617	1.2915
KF	17.710 70	2.972 55	5.918 43	2.647 84	0.2156	1.4004
KCl	17.476 90	2.960 61	6.759 74	2.215 35	0.2395	1.2672
KBr	22.050 13	3.054 80	5.701 99	2.002 52	0.3509	1.2096
KI	25.744 48	3.110 93	4.980 11	1.798 41	0.4462	1.1396
RbF	19.639 51	2.744 99	6.395 04	2.683 66	0.2108	1.3570
RbCl	20.273 84	2.751 18	6.931 90	2.224 32	0.2584	1.2299
RbBr	25.096 59	2.829 42	5.859 06	2.011 82	0.3709	1.1758
RbI	28.703 50	2.873 18	5.021 59	1.801 39	0.4728	1.1072

[a] All data in atomic units. $t_1 = (\alpha + \beta)^{-1} \ln(a\alpha/b\beta)$, $t_2 = (\alpha\beta)/(\alpha + \beta)$

If we express this last relation in crystallographic coordinates

$$\bar{x}_b = \frac{\beta}{\alpha+\beta} + \frac{1}{r_{ca}(\alpha+\beta)} \ln \frac{a\alpha}{b\beta} \tag{3}$$

The crystallographic position of the *b*-point is, therefore, inversely proportional to the bond distance. If we make another reasonable assumption, that $a\alpha$—being associated with a difficult to deform, or hard, cation—is larger than $b\beta$, we see that the slope in this expression should be positive, in complete agreement with our findings.

Substituting eq 2 into eq 1 we obtain in a straightforward manner

$$\ln \rho = -\frac{\alpha\beta}{\alpha+\beta} r_{ca} + \ln k \tag{4}$$

$$k = a\frac{\alpha+\beta}{\beta} \exp\left(-\frac{\alpha}{\alpha+\beta} \ln \frac{a\alpha}{b\beta}\right) \tag{5}$$

which indicates the proportionality of the logarithm of the density to the bond distance. In a similar way we may conclude that, to first order

$$\ln(\nabla^2\rho) = \ln \rho + \ln(\alpha\beta) \tag{6}$$

the logarithm of the Laplacian at the *b*-point being just a displaced logarithm of the density.

It is interesting to examine the model in a more systematic way. To determine these parameters accurately, we have obtained both the cation−anion *b*-point position and the electron density at the *b*-point for all noncesium alkali halides at several lattice parameters expanding a range $a = a_{exp} \pm 0.5\ a_0$, where a_{exp} is the experimental parameter. These data have been fitted linearly to eqs 2 and 4 to obtain the a, α and b, β pairs. We have obtained in every case a regression coefficient better than 0.999 98. The results are shown in Table 3.

The table shows that all the parameters evolve smoothly with both the cation and anion, except the fluoride salts that display the well-known head of group anomaly. In this way, the α, β parameters decrease at constant cation with the size of the anion, and at constant anion with the size of the anion. The a, b pair evolves differently on going down in a group at constant anion. The a parameter increases, while the b parameter decreases. These findings are compatible with assigning to the exponential parameters the meaning of "hardness" that is so common in chemistry. Cations are, therefore, harder than anions, except perhaps Rb^+ in RbBr and RbI as compared to F^- in LiF. Moreover, our data shows that the hardness of a cation *in a crystal* increases as the hardness of the anion decreases, except in the fluorides. The behavior of the anions is a little more complex, but there is a strong tendency toward constant β as the anion size grows. For example, the I^- hardness is only 0.15 units larger in LiI than in RbI. It is also to be noticed that the fifth column of Table 3 is the slope of eq 3 as a linear relation between $\bar{x}_b$ and $1/r_{ca}$, determining the relative compressibility of cations versus anions. This shows how the cations in fluorides grow in relative size with respect to the anions less than in the rest of the halides on compression. Bigger cations, like K^+, or Rb^+, display the largest variations in relative size with respect to anions. This fact, together with the relative constancy of their radii, allows us to describe these cations as sticky spheres. Finally, the last column of Table 3 is the negative of the slope in eq 4. It describes how quickly the density at the *b*-point separates from its equilibrium value on variation of the lattice parameter and is, therefore, a possible measure of bond strength.

It is possible to relate the values of α, β to effective orbital exponents. In the lithium case, where only 1s functions are employed, this is straightforward. We have obtained a mean effective charge in lithium compounds $Z^* = 2.7234$, in excellent agreement with that obtained from Slater's rules.[47] Moreover, it is known that the tail of isolated atomic densities behaves asymptotically as $\exp(-\sqrt{(8\epsilon)})$, where ϵ is the orbital energy of the highest occupied atomic orbital. We have found a good linear relation between our α, β values and $\sqrt{(8\epsilon)}$, with correlation coefficients greater than 0.98. In recent work[32] Ghanty and Ghosh have used the "density exponent" $|\nabla\rho|/\rho$, calculated at the classical turning points in pseudopotential calculations in free atoms and ions, to define a new scale of orbital radii à la Zunger. They have successfully related both the radii and exponent with almost every atomic property (electronegativity, polarizability, etc). From eq 1 we see that this coefficient is almost identical with our α's and β's to the left or to the right, respectively, of the *b*-point. Our coefficients are, however, obtained in actual crystals, showing a richer structure.

The tail model helps us explain a large part of our results. Nevertheless, it is not enough to understand the linear relations in Figure 6. It may be shown that the straight lines of eq 2 have definitely greater slopes than the constant cation slopes of the figure. We think that the linearity observed has its roots in a characteristic periodic variation of α, β and the cell parameter of the lattices, very likely related to the nuclear charge Z.

5. Ionic Radii and Linear Correlations

We will devote this section to the examination of several known correlations among ionic radii and different atomic properties in light of the AIM theory. The results, together with some definitions that are particular to the theory, will guide us to discover new interesting relations that widen the significance of the ionic radius concept.

A. Bonding. Bonding in ionic crystals has received much less interest through the years than it deserves. It has been usual to think of it as the result of a balance between classical Coulombic forces among point charge ions and "quantum mechanical" repulsions. However, it hides a wealth of interesting features. There have been two main streams in this topic. On one hand, a basically energetic school has focused on the

TABLE 4: Electron Densities and Laplacians at the Cation−Anion and Anion−Anion *b*-Points (If Present) for the B1 Phases of the Alkali Halides at the Experimental Geometries[a]

system	$\rho_{ca.}$	$\nabla^2\rho_{ca.}$	ρ_{aa}	$\nabla^2\rho_{aa}$
LiF	1.710×10^{-2}	1.710×10^{-1}	8.534×10^{-3}	5.002×10^{-2}
NaF	1.705×10^{-2}	1.368×10^{-1}	2.995×10^{-3}	1.984×10^{-2}
KF	1.674×10^{-2}	9.250×10^{-2}		
RbF	1.633×10^{-2}	8.328×10^{-2}		
CsF	1.630×10^{-2}	6.838×10^{-2}		
LiCl	7.641×10^{-3}	6.600×10^{-2}	6.124×10^{-3}	2.536×10^{-2}
NaCl	9.433×10^{-3}	6.441×10^{-2}	3.084×10^{-3}	1.236×10^{-2}
KCl	1.072×10^{-2}	5.117×10^{-2}		
RbCl	1.062×10^{-2}	4.702×10^{-2}		
LiBr	6.709×10^{-3}	5.327×10^{-2}	6.615×10^{-3}	2.216×10^{-2}
NaBr	8.489×10^{-3}	5.273×10^{-2}	3.427×10^{-3}	1.235×10^{-2}
KBr	1.015×10^{-2}	4.371×10^{-2}	1.409×10^{-3}	6.137×10^{-3}
RbBr	1.003×10^{-2}	4.005×10^{-2}		
LiI	5.497×10^{-3}	3.981×10^{-2}	6.753×10^{-3}	1.765×10^{-2}
NaI	6.967×10^{-3}	3.931×10^{-2}	3.694×10^{-3}	1.076×10^{-2}
KI	8.708×10^{-3}	3.386×10^{-2}	1.631×10^{-3}	5.817×10^{-3}
RbI	8.845×10^{-3}	3.172×10^{-2}	1.136×10^{-3}	4.386×10^{-3}

[a] All values in atomic units.

relative importance of the different contributions to cohesion,[48] the role of van der Waals forces,[34] the influence of charge transfer on total energy pseudopotential calculations,[21] etc. When trying to rationalize these results, concepts such as ionicity[49] or covalence[50] have always been controversial. All of these approaches lie usually within the chemical concept of *bonding* in the energetic sense, but outside that of *bond*, which is firmly connected with geometry. In this last sense, much less work has been actually done, and Pauling's bond valence, with some reformulations and modifications, is still a rather valid reference (see ref 51 for a review).

In the context of the AIM theory,[35] bonding is particularly related to the Laplacian of the electronic density. It has been nicely shown how this new scalar field, which measures the local accumulation of electronic charge, is related to the different types of atomic interactions and to the valence shell electron pair repulsion model (VSEPR). In our context, it is particularly important to realize that positive Laplacians in the bonding region (and particularly at the *b*-point) are related to closed-shell interactions, while the contrary is true for shared (or covalent) interactions. Charge depletion in Berlin's binding regions[52] destabilizes the nuclear configuration, while charge concentration stabilizes it, leaving charge transfer and dispersion as main responsibles for cohesion in closed-shell systems. In this manner, a geometrical model recovers the energetic features of bonding. It is well-known that bonding in alkali halide diatomic molecules is of the closed-shell type, as well as in noble gas dimers. However, there appear to be subtle differences in the Laplacians of both types of systems. In noble gas dimers, the *b*-point in ρ corresponds to a maximum of $\nabla^2\rho$ (minimum of $-\nabla^2\rho$), the latter property being better suited to study charge concentrations and depletions. In ionic systems, however, a *b*-point in ρ usually corresponds to a saddle point in $\nabla^2\rho$, implying a certain tendency toward sharing interactions.

We have found a positive $\nabla^2\rho$ value at every *b*-point examined, not only in alkali halides but in all the 120 perovskites, the 20 alkaline earth halide fluorites, etc. The *b*-point Laplacians for the B1 alkali halides at the experimental geometries are summarized in Table 4. It is seen how they are mainly organized by anions and how the fluorides give the tightest values. It is also to be noticed that the absolute values of $\nabla^2\rho$ in these systems are extremely small as compared with those of shared interactions, being in the anion−anion cases

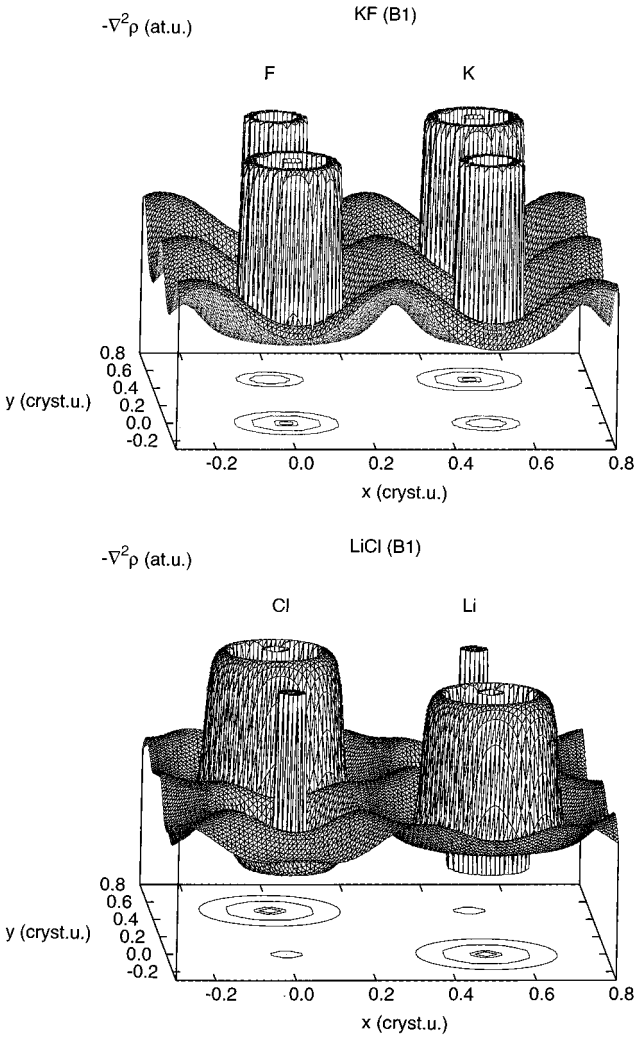

Figure 8. $-\nabla^2\rho$ surfaces on the [001] plane of two B1 alkali halides: (a, top) KF, (b, bottom) LiCl. Only four coplanar ions (two cations and two anions) are shown in each plot. Anions are located at the top left−bottom right diagonal ends, and cations at the bottom left−top right ones. The (0.25, 0.25, 0) crystallographic point is located at the center of both diagonals. The Laplacians have been clipped at values equal to ± 0.8 au. The *z* scale has been modified according to the arctangent function to reinforce the visibility of the chemical interesting region of $\nabla^2\rho \approx 0$. $\nabla^2\rho = 0$ isolines have also been projected onto the *xy* plane.

somewhat smaller than in the cation−anion ones, but of the same order of magnitude. Therefore $\nabla^2\rho$ cannot be relied upon to distinguish clearly between cation−anion and anion−anion bonds.

A much more detailed view of the bonding properties is given in Figure 8. In it we plot minus the Laplacian surface on the [100] plane in B1 KF and LiCl. The surface is always negative in the bonding regions, but there is a clear region of smaller charge depletion over the cation−anion bonds, as $-\nabla^2\rho$ is a maximum along the bond line and a minimum in the orthogonal direction. This topology of the ionic bonds has turned out to be independent of the system studied. Out of the two cases displayed, KF is a (2111) system at the experimental geometry and does not display a topological anion−anion bond. In its place there is a ring point, which, from examination of the $-\nabla^2\rho$, is a region of much lesser charge depletion than its surroundings. On the contrary, LiCl is a (2222) system, and there is a clear anion−anion topological bond, with the same characteristics shown by the Li−Cl one. This bond forces a saddle in $-\nabla^2\rho$ at (0.25, 0.25, 0) and two local concentration regions near the

alkali ions, which coincide approximately with the two new ring positions. These patterns have been previously reported[19] in a very interesting experimental determination of the electron density of the mineral danburite, using an aspherical refinement of the empirical data. We feel that this fact is an independent support of our results. These are rather remarkable findings and seem to indicate that ring points in ionic systems constitute regions of a small, but clear, decrease of the general charge depletion that bonding regions display. In our opinion, their role in bonding should be further examined. A conclusion of this work is that ionic bond in crystals is a closed-shell interaction with peculiar characteristics not present in van der Waals complexes.

If ionic bonding behaves as all known bonds, it should display the same type of correlations shown by other interactions. In our context, bond strength−bond length relations are the most representative ones. They have been known for years and are the cornerstone of modern structural studies. In the AIM theory, it was soon established that the charge density at a *b*-point was clearly related to the bond length (see, for example, ref 55). There have been, however, quite a different number of proposals about the functional relationship between the two magnitudes. For example, Bader himself[55] proposed a linear relation between ρ_b and r_b, where the subindex *b* refers to properties at the *b*-point. More recently, Knop, Boyd, and Choi[56] used a power law, $r_b = k\rho_b^{-\gamma}$, to fit S−S densities and bond distances in a series of sulfur compounds. They reasoned that the true relation should fulfill the correct infinite limit ($\rho \rightarrow 0$, $r_b \rightarrow \infty$) and that Bader's linearity did not. They also realized that, given the often reduced range of distances spanned by the experimental bond lengths, many different functional forms might fit the same set of data. In our opinion, an exponential form, $\rho_b = K \exp(-\gamma r_b)$, is more justifiable from the theoretical point of view. We have fitted again both Bader's and Boyd's data to this expression and obtained as good agreements as those found with their own functions. This seems to indicate that normal covalent bonds in isolated molecules actually display the same properties as those derived from our tail model. The electron density near the *b*-point in a covalent bond is not as easily imagined as the overlap of two exponentials, like in the ionic case. Nevertheless, it has been proven[46] that Slater's[57] old conjecture, stating that the electron density in a bonded system should be hardly different from the superposition of free atomic densities, gives rise to calculated bonded radii (promolecule or procrystal radii) matching the X-ray radii within 0.04 a_0. In a similar manner, bond order has been related to densities at the *b*-point. In this case, Bader has shown that in C−H single bonds, accepted bond orders (λ) grow exponentially with increasing densities, $\lambda = A \exp(B\rho_b)$. It is easily seen that this expression has also an incorrect limit for vanishing density. We have found that a very good fitting is also obtained with his data if they are approximated to a potential form, $\lambda = k\rho^N$, which displays an appropriate limit.

In molecular chemistry language, therefore, bond length immediately evokes bond strength or bond order. In crystalline systems, however, changes in interionic distances are usually related to changes in coordination and not connected to bond strength. In this sense, Pauling's[8] bond valence is perhaps one of the few indices with a certain strength content. It was originally defined as $s = q/n$, where q is the nominal charge of the ion and n its coordination index. According to Pauling's rules, a change in the coordination of an ion induces a change in its bond valence, which through a simple energetic model (like a Born−Mayer expression) may be straightforwardly connected to a change in interionic distance. These ideas have been improved over the years, and Brown et al.[22,23] have proposed potential ($s = Ar_b^{-N}$) or exponential ($s = A \exp(-Br_b)$) formulas, where N, A, B are suitable constants for a particular atom pair. With them, they have obtained extremely successful versions of the law of constancy of valence.

Taking into account eq 4 of the tail model and making the supposition that bond valence means nothing but bond order in ionic systems, we can use the previous relation $\lambda = k\rho^N$ to recover the exponential variation of s with r_b, supported both in molecular and solid-state chemistry. Moreover, except the values of k and N, which are fixed by convention, all the other parameters are contained in the tail model. Bond valence *is* bond order, and bond distance variations due to intercompound or coordination changes are to be associated with changes in bond strength, using the same tools used to study covalent interactions. The sometimes disconcerting variability of radii displayed by ionic compounds should be seen as a result of the very different effective bond valences found in crystals.

Figure 9 shows the linear ρ_b versus $r_{ca.}$ relation obtained in cation−anion bonds for all the 160 compounds studied, plus the alkali halide diatomic molecules, at the theoretical equilibrium geometries. Each line shows the evolution of a particular bond (Li, Be−F at the upper left corner and Cs, Ba−I at the lower right one). It is remarkable how a change in coordination is completely equivalent to a change of distance when in the perovskites we change the structure by maintaining divalent cations and anions and changing the univalent alkali ion. It is also interesting that the slopes in this plot are all within a very small window, indicating a single bond family. Using mean values, our B2 cationic radii are 1.02−1.04 times larger than those in the B1 structure, to be compared with Pauling's ratio, equal to 1.036. In the same way, 8-fold coordinated fluorite cations are 1.05−1.06 times bigger than in the 6-fold coordinated perovskite structure. These results should be taken with care, since the geometries used are theoretical, but show the consistency of our approach with general theories of bonding. Average cationic and anionic bonded radii are shown in Figure 10. Pauling's proportionality of radii with coordination index is particularly striking. Though the constants relating the several radii at several coordination indices are not those of Pauling and depend slightly on the type of compound (going from coordination six to eight scales radii differently in the B1 to B2 case than in the perovskite to fluorite one), it is rather interesting that equilibrium distances of different phases display such simple correlations. This fact supports considering bonds differing in coordination as different bond order flavors of the same bond.

B. Electronegativity and Deformability. Electronegativity (χ) is another of the concepts that has played a prominent role in the theory of the ionic bond. The very word is usually associated with Pauling,[58] though a large number of people have contributed through the years to enlarge its meaning. Literally hundreds of works have been devoted to this concept in the last 60 years, particularly in the chemical literature. It has been shown by statistical factor analysis[59] that all the ionicity measures that have been proposed display only a single principal component that covers more than 90% of the variances. The different electronegativity scales are just different ways to measure it. Almost 10 years ago Allen[60] showed that χ may be easily defined as the average one-electron energy of the valence shell electrons of neutral atoms. In our HF frame, we have found that any of the common χ scales, but particularly those of Pauling and Allred-Rochow,[61] correlate linearly with

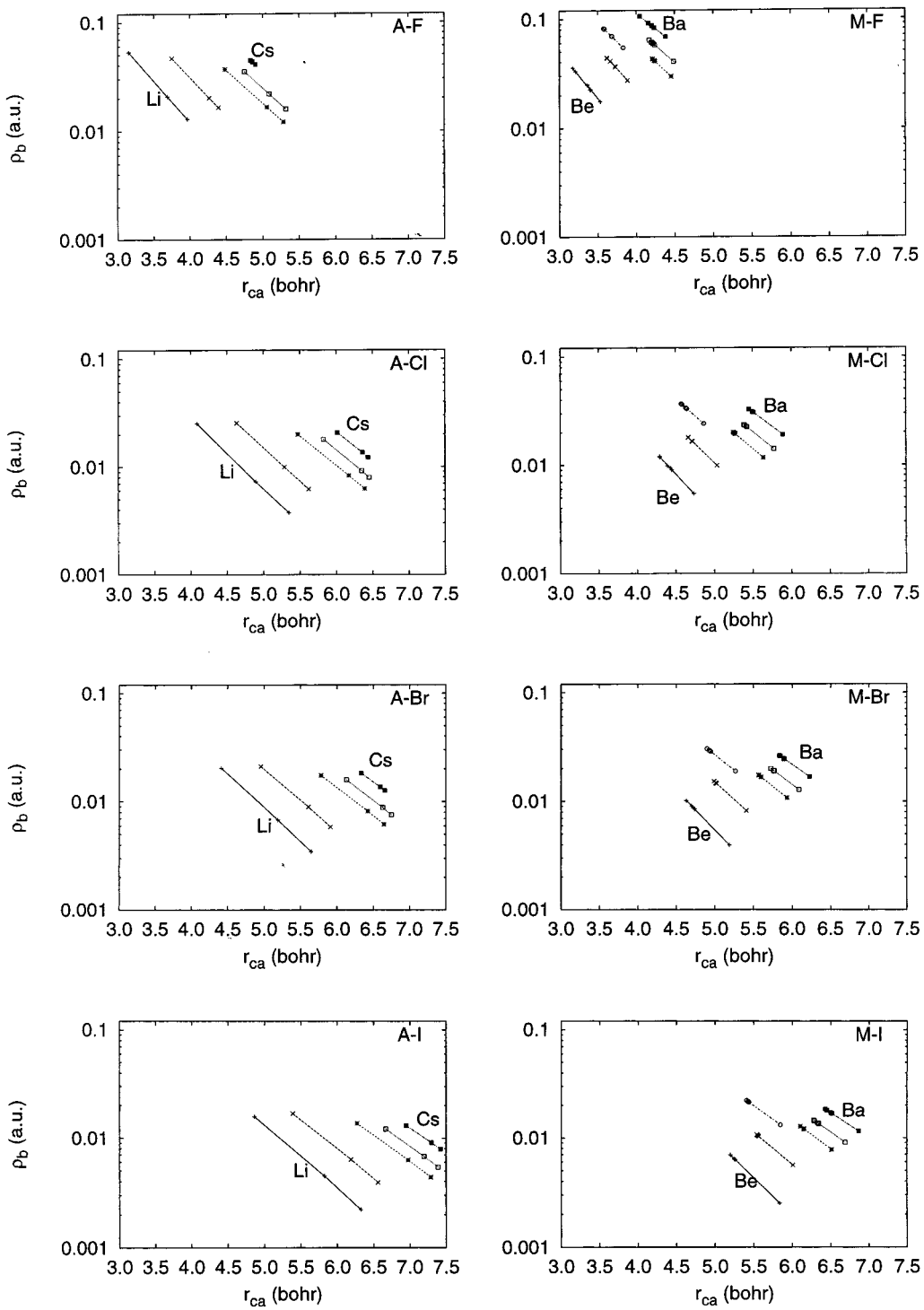

Figure 9. $\rho_b - r_{ca}$ relation for the cation−anion bonds in the compounds studied in this work. Each plot displays a family of bonds that share a common anion while differing in the cation. They are easily identified from the top-left label. The A symbol stands for the Li−Cs series of alkali cations and the M symbol for the Be−Ba series, with Zn between Mg and Ca. As the alkali−halide bonds are concerned, the three density points per type of bond come from the diatomic molecules and the B1 and B2 crystalline phases calculated at the HF+CEC geometries. Notice how changes in coordination (2, 6, 8, respectively) are accompanied by changes in distance and density. The alkaline earth−halide bonds include density points calculated at the HF+CEC geometries from all AMX_3 and MX_2 compounds that display those bonds. The density scale is logarithmic.

the orbital energy of the highest occupied atomic orbital (HOAO), ϵ_{orb}, of neutral atoms. We have also found that ϵ_{orb}'s for the fundamental states of alkali cations, alkaline earth cations, and halide anions are also linearly proportial to their corresponding ϵ_{orb}'s of the neutral species. This means that our tail model parameters, related to orbital energies in crystals, must show a clear relation to electronegativity.

Such a program has been carried out by Boyd et al.,[62] who have devised an electronegativity scale for atoms and groups of atoms based upon the properties of the electron density at the AIM *b*-point. Following reasonable arguments, they construct a scalar proportional to the asymmetry of the *b*-point in a series of diatomic hydrides, and inversely proportional to the number of valence electrons and to the density at the critical point. Fitting a potential function of this scalar to Pauling's scale (referred to hydrogen), they found excellent correlations, demonstrating that the properties of the critical point were immediately related to the difference of electronegativity

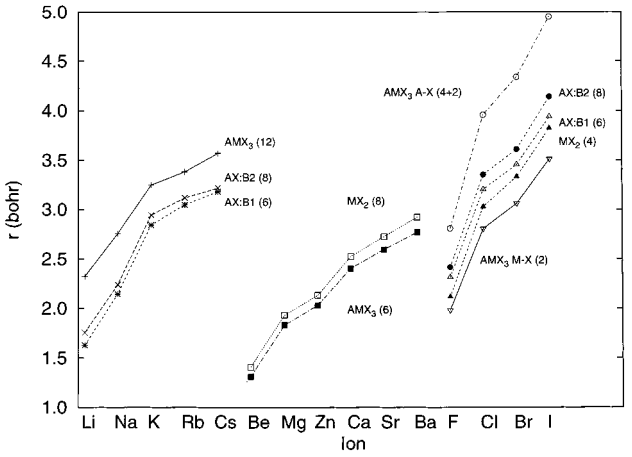

Figure 10. Average cationic and anionic radii at the theoretically determined equilibrium geometries. A stands for the alkali ions, M for the alkaline earth cations, and X for the halide anions. When several bonds are possible, the specific type of bond is shown. Numbers to the right of the labels correspond to classical coordination indices.

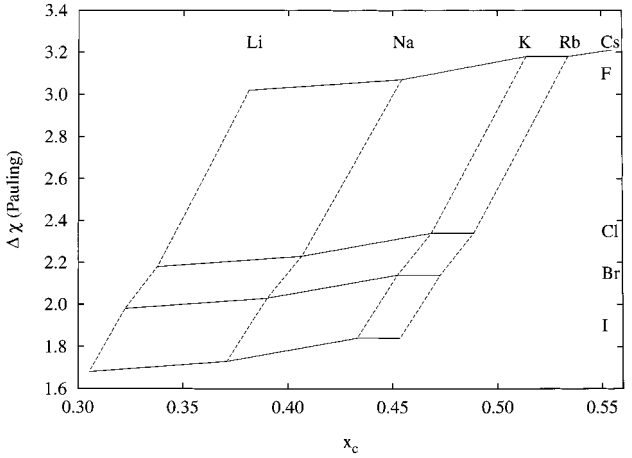

Figure 11. Variaton of the difference of cation and anion electronegativity in Pauling's scale ($\Delta\chi$) with the relative position of the cation−anion bond point ($x_c = r_c/r_{ca}$) in the B1 alkali halides at the experimental geometries.

between the bonded atoms. Figure 11 shows how this relation is also fulfilled using crystalline *b*-points. It is to be noticed that linearity is obtained with any of the ions acting as the reference from which to measure χ. For a constant cation, the effect of a change of anion in the relative size of the cation−anion pair is the same as a scaled change in electronegativity. Moreover, going from iodide to fluoride involves a change in the relative size of ions almost independent of the specific cation. Running over the cations at constant anion implies a change of 0.16 units in $\Delta\chi$ and almost a constant change of 0.15 units in x_c.

We have examined a certain number of magnitudes with respect to a plausible relation to electronegativity changes. In most cases, χ may play the same role as ionic radius, and many of the figures already presented in this paper have a correlate in terms of χ. We will concentrate therefore on new concepts. Ionic deformation and deformability have usually been associated with polarizability or with ionic hardness. We have already introduced hardness in our discussion as a difficulty in changing *b*-point positions, but there is a genuinely geometric definition in the AIM context. The difference in shape of an atomic (ionic) basin with respect to a sphere is a clear and measurable concept. To simplify as much as possible, we may introduce a single scalar magnitude, δ, the ratio of the ionic radius along the

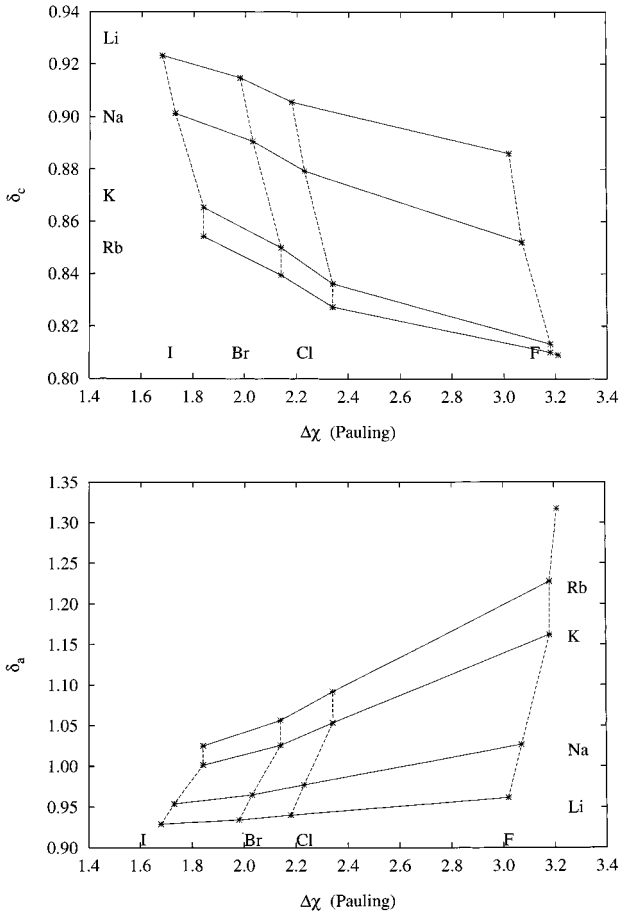

Figure 12. Cationic (a, top) and anionic (b, bottom) deformations (see text) versus $\Delta\chi$ in B1 alkali halides at experimental geometries.

cation−anion bond direction (the tightest one), and the mean ionic radius, $\delta = r_c/r_{c,mean}$. Mean radii have been obtained by calculating the volume of the atomic basins and simulating it by a sphere. We have found that mean radii are proportional to bonded radii. For example, the alkali halide cations in the B1 phase fulfill extremely well the following equation: $r_{c,mean} = 1.30r_c - 0.315$, where distances are measured in a_0. Figure 12a shows the deformations of cations in the B1 alkali halides as a function of $\Delta\chi$. It is clear, on one hand, that deformability grows as the cationic size grows, and that big cations, like rubidium, spread all over greater regions than small ones. On the other hand, cationic deformation is quite dependent on the anion, the fluoride being the most distorting one. This view is in complete agreement with intuition and chemical background. As anions are concerned, we have not been able to obtain such a simple relation between the ratio of anionic radii along cation−anion bonds to mean anionic radii and χ. However, simplicity is recovered if the relevant radius used to define the deformation is not the cation−anion bond one, but the anion−anion contact radius, r_{aa}. Doing so, and defining $\delta_a = r_{aa}/r_{a,mean}$, we obtain Figure 12b. It is observed that δ_a is greater than one for potassium and rubidium salts, and smaller for lithium and sodium compounds. This means that Li and Na halides display strained anions, since the anion−anion direction is particularly unfavorable from the energetic point of view. We will exploit this and other ideas in upcoming papers of this series. Anyway, deformation of anions seems to be virtually a function of the countercation, lithium salts giving the most deformed anions. For a given cation, deformability of the different anions seems to be rather similar, with a slight tendency for softness on increasing anionic size.

We think that these data, perfectly compatible with classical geometrical thinking in physics and chemistry, should play a role in introducing the AIM methods in solid-state science.

6. Conclusions

We have shown in this paper how the application of the AIM theory to ionic compounds is able to illuminate the traditional concept of ionic radius. On one hand, the theory uncovers the complexity and richness of atomic or ionic shapes in the crystalline state, as exemplified in our previous papers, and in the present analysis of the B1 and B2 phases of the alkali halides. New ideas, like the possibility of color topologies or pressure-induced topological isomerizations, have been presented, opening the way to very likely interesting effects, which should be further studied.

On the other hand, this same complexity, clearly and objectively defined, may be used to understand several known behaviors of ionic radii and to guide us to discover others. In this sense, we have shown that the theory of bonding in ionic materials is based on the same grounds as in covalent molecular systems. Pauling's bond valence concept has turned out to be a scaled bond order, and the variation of ionic radii with coordination index may be traced to changes in bond strength.

Many well-known atomic or ionic properties, like electronegativity, also find their place in the theory, being related to measurable magnitudes at the AIM *b*-points. Moreover, some other entities, as the atomic hardness, may be related to actually geometrical ideas, like the deformation of the atomic basins, creating a particularly easy to grasp image of their associated phenomena.

The occurrence of so many relationships among the topological ionic radii and the topological properties evidences the geometric nature of binding in crystals. Given the high anisotropy of atomic basins, even the bizarre shape of some of them, it may appear shocking to use the topological radii as a measurement of ionic size. This is, however, a direct consequence of the importance of *b*-points in determining crystal properties. The surprise is to observe that a thorough knowledge of the electron density properties in a reduced set of points is enough to rationalize microscopic and macroscopic crystal properties, although generally we need to determine the electron density on the whole crystal before knowing where those points are located.

Finally, we think that there is still plenty of room in solid-state science for stimulating ideas coming from Bader's theory. The geometrization of nature is an ever active program that is followed pleasantly by our minds. It is worthwhile to continue along these lines.

Acknowledgment. We are grateful to the Spanish Dirección General de Investigación Científica y Técnica (DGICYT), Project No. PB96-0559, for financial support.

References and Notes

(1) Landé, A. *Z. Phys.* **1920**, *1*, 191.
(2) Wasastjerna, J. A. *Soc. Sci. Fenn., Commentat. Phys.-Math.* **1923**, *38*, 1.
(3) Goldschmidt, V. M. *Skr. Nor. Vidensk. Akad., Kl. 1; Mat-Naturvidensk. Kl.* **1926**, *2*; *Chem. Ber.* **1927**, *60*, 1263.
(4) Pauling, L. *Proc. R. Soc. London A* **1927**, *114*, 181; *J. Am. Chem. Soc.* **1927**, *49*, 765.
(5) Zacharasen, W. H. *Z. Kristallogr.* **1931**, *80*, 137.
(6) Pauling, L. *Z. Kristallogr.* **1928**, *67*, 377.
(7) Huggins, M. L. *J. Chem. Phys.* **1937**, *5*, 143.
(8) Pauling, L. *The Nature of the Chemical Bond*; Cornell University Press: Ithaca, NY, 1960.
(9) Pauling, L. *J. Am. Chem. Soc.* **1929**, *51*, 1010.
(10) Fumi, F. G.; Tosi, M. P. *J. Phys. Chem. Solids* **1964**, *25*, 31. Tosi, M. P.; Fumi, F. G. *J. Phys. Chem. Solids* **1964**, *25*, 45.
(11) Witte, H.; Wölfel, E. *Z. Phys. Chem.* **1955**, *3*, 296.
(12) Schoknecht, G. *Z. Naturforsch.* **1955**, *129*, 983.
(13) Shannon, R. D.; Prewitt, C. T. *Acta Crystallogr.* **1978**, *B25*, 1965.
(14) Boswara, I. M. *J. Phys. Chem. Solids* **1981**, *42*, 487.
(15) Baert, F.; Coppens, P.; Stevens, E. D.; Devos, L. *Acta Crystallogr.* **1982**, *A38*, 143.
(16) Hirscheld, L.; Hope, H. *Acta Crystallogr.* **1980**, *B36*, 406.
(17) Geisinger, K. L.; Spackman, M. A.; Gibbs, G. V. *J. Phys. Chem.* **1987**, *91*, 3237.
(18) Coppens, P. *Annu. Rev. Phys. Chem.* **1992**, *43*, 663.
(19) Downs, J. W.; Swope, R. J. *J. Phys. Chem.* **1992**, *96*, 4834.
(20) O'Keeffe, M. In *Structure and Bonding in Crystals*; O'Keeffe, M., Navrotsky, A., Eds.; Academic Press Inc: New York, 1981; Vol. II.
(21) Chelikowsky, J. R. *Phys. Rev.* **1986**, *B34*, 5295.
(22) Brown, I. D. *Acta Crystallogr.* **1977**, *B33*, 1305.
(23) Brown, I. D.; Alternatt, D. *Acta Crystallogr.* **1985**, *B41*, 244.
(24) Zunger, A.; Cohen, M. L. *Phys. Rev.* **1979**, *B19*, 4082.
(25) Zunger, A. *Phys. Rev.* **1980**, *B22*, 5839.
(26) Simons, G.; Bloch, A. N. *Phys. Rev.* **1973**, *B7*, 2754.
(27) St. John, J.; Bloch, A. N. *Phys. Rev. Lett.* **1974**, *33*, 1095.
(28) Machling, E. S.; Chow, T. P.; Phillips, J. C. *Phys. Rev. Lett.* **1977**, *38*, 1292.
(29) Chelikowsky, J. R.; Phillips, J. C. *Phys. Rev.* **1978**, *B17*, 2453.
(30) Villars, P. J. *Less-Common Met.* **1983**, *92*, 215; **1984**, *99*, 33; **1984**, *102*, 199.
(31) Zhang, S. B.; Cohen, M. L. *Phys. Rev.* **1989**, *B39*, 1077.
(32) Ghanty, T. K.; Ghosh, S. K. J. *Phys. Chem.* **1996**, *100*, 17429.
(33) Bucher, M. *Phys. Rev.* **1983**, *B27*, 5919.
(34) Bucher, M. *Phys. Rev.* **1987**, *B35*, 5985.
(35) Bader, R. F. W. *Atoms in Molecules*; Oxford University Press: Oxford, 1990.
(36) Martín Pendás, A.; Costales, A.; Luaña, V. *Phys. Rev.* **1997**, *B55*, 4275.
(37) Luaña, V.; Costales, A.; Martín Pendás, A. *Phys. Rev.* **1997**, *B55*, 4285.
(38) Luaña, V.; Pueyo, L. *Phys. Rev.* **1990**, *B41*, 3800.
(39) Luaña, V.; Martín Pendás, A. J. M.; Recio, Francisco, E.; Bermejo, M. *Comput. Phys. Commun.* **1993**, *77*, 107.
(40) Recio, J. M.; Martín Pendás, A.; Francisco, E.; Flórez, M.; Luaña, V. *Phys. Rev.* **1993**, *B48*, 5891, and references therein.
(41) Martín Pendás, A. The CRITIC program, 1995. The code is available upon request. Contact the author at e-mail: angel@fluor.quimica.uniovi.es.
(42) Chakravorty, S.; Clementi, E. *Phys. Rev.* **1989**, *A39*, 2290.
(43) *Handbook of Chemistry and Physics*, 64th ed.; Weast, R. C., Ed.; Chemical Rubber Co.: Boca Raton, FL, 1983−1984.
(44) Clementi, E.; Roetti, C. *At. Data Nucl. Data Tables* **1974**, *14*, 177.
(45) Koga, T.; Watanabe, S.; Kanyayama, K.; Yasuda, R.; Thakkar, A. J. *J. Chem. Phys.* **1995**, *103*, 3000.
(46) Feth, S.; Gibbs, G. V.; Boisen, M.; Myers, R. H. *J. Phys. Chem.* **1993**, *97*, 11445.
(47) See for example: Levine, I. N. *Quantum Chemistry*, 4th ed.; Prentice-Hall: Englewood Cliffs: NJ, 1991.
(48) Majewski, J. A.; Vogl, P. *Phys. Rev. Lett.* **1986**, *57*, 1366.
(49) Phillips, J. C. *Rev. Mod. Phys.* **1970**, *42*, 317.
(50) Adachi, H. J. *Phys. Soc. Jpn.* **1993**, *62*, 3965.
(51) Burdett, J. K. *Chem. Rev.* **1988**, *88*, 3.
(52) Berlin, T. J. *Chem. Phys.* **1951**, *19*, 208.
(53) Luaña, V. The TESSEL program, 1997. Contact the author at victor@carbono.quimica.uniovi.es or check http://www.uniovi.es/~quimica.fisica/qcg/tessel.html.
(54) Phillips, M.; Munzner, T.; Levy, S. GEOMVIEW, 1995, available via anonymous ftp from geom.umn.edu. The Geometry Center at the University of Minnesotta.
(55) Bader, R. F. W.; Tang, T. H.; Tal, Y.; Biegler-König, F. W. *J. Am. Chem. Soc.* **1982**, *104*, 946.
(56) Knop, O.; Boyd, R. J.; Choi, S. C. *J. Am. Chem. Soc.* **1988**, *110*, 7299.
(57) Slater, J. C. *Quantum Theory of Molecules and Solids*; McGraw-Hill, New York, 1965.
(58) Pauling, L. *J. Am. Chem. Soc.* **1932**, *54*, 3570
(59) Meister, J.; Schwarz, W. H. E. *J. Phys. Chem.* **1994**, *98*, 8245.
(60) Allen, L. C. *J. Am. Chem. Soc.* **1989**, *111*, 9003.
(61) Allred, A. L.; Rochow, E. G. J. *Inorg. Nucl. Chem.* **1958**, *5*, 264.
(62) Boyd, R. J.; Edgecombe, K. E. *J. Am. Chem. Soc.* **1988**, *110*, 4182. Boyd, R. J.; Boyd, S. L. *J. Am. Chem. Soc.* **1991**, *114*, 1652. Komorowski, L.; Boyd, S. L.; Boyd, R. J. *J. Phys. Chem.* **1996**, *100*, 3448.